https://doi.org/10.46813/2025-160-076

STRUCTURAL AND PHASE TRANSFORMATIONS IN A MOLYBDENUM TARGET UNDER THE IMPACT ACTION OF A HIGH-POWER ELECTRON BEAM

V.V. Bryukhovetsky[1], S.E. Donets[1], S.A. Kniaziev[2], O.V. Subbotin[2], V.V. Lytvynenko[1], S.I. Bogatyrenko[4], O.L. Rak[3], A.R. Shymanovskyi[4]
[1]Institute of Electrophysics and Radiation Technologies NAS of Ukraine, Kharkiv, Ukraine;
[2]National Technical University "Kharkiv Polytechnic Institute", Kharkiv, Ukraine;
[3]NSC "Kharkiv Institute of Physics and Technology", Kharkiv, Ukraine;
[4]V.N. Karazin Kharkiv National University, Kharkiv, Ukraine
E-mail: vvlytvynenko@ukr.net

The paper studies the features of surface relief, structure and orientation of grains in the surface layer, structural and phase composition, and microhardness of a molybdenum target irradiated with a high-current pulsed electron beam (HCEB). The effect of columnar grain surface microstructure formation by epitaxial growth from the substrate has been established. Temperature field distribution modelling has been performed, showing that temperature gradients along the surface cause instabilities in the molten layer, which lead to the formation of dissipative structures.

PACS: 52.40.HF, 29.27Ac, 621.715:539.376, 87.55N

INTRODUCTION

Molybdenum has a number of applications due to its high heat resistance and radiation resistance [1-5], which stimulates research aimed at establishing the limits of its operational characteristics under the influence of concentrated energy flows on the material.

In [1], it is noted that under the highly intensive influence of compression plasma on molybdenum, a sub-grain structure is formed due to the Bénard–Marangoni effect, which in turn arises due to the temperature gradient across the target surface. At the same time, the remelted surface layer is characterized by the formation of a columnar structure. Regarding the change in microhardness, the authors conclude that two competing processes are at work here. The formation of a subgrain structure contributes to an increase in microhardness, while the formation of a columnar structure causes it to decrease. Comparing the state of the molybdenum and tungsten surfaces, it is noted that macro-cracks form in tungsten due to the mechanism of internal stress generation, while micro-cracks occur in molybdenum as a result of resolidification processes. Paying attention to these mechanisms, it should be noted that in the case of plasma compression flow treatment, the maximum energy release will occur on the surface, whereas in the case of electron beam application, this maximum will be shifted to the subsurface region. And with a comparable power flow, a greater variety of both destructive and modifying processes can be expected. Such temperature unevenness should also be more clearly reflected in the manifestation of the Bénard–Marangoni effect.

Molybdenum is also used in elementary particle physics experiments as a spallation target and beam intercepting devices, but the material must also meet radiation and thermal stability requirements, as its temperature rises to over 900 °C, as investigated in [2]. At the same time, more extreme conditions of radiation and thermal stress, which can occur during the operation of accelerators, can be reproduced using a high-current relativistic electron beam.

Molybdenum is also used as a target for the production of medical isotopes, and therefore it is also necessary to assess the stability of its mechanical characteristics and the preservation of its integrity under conditions of simultaneous radiation heating and forced cooling [3]. Since conditions for the occurrence of a temperature gradient were created to establish the operational limits of the integrity of the molybdenum target, the use of a pulsed radiation source will make it possible, thanks to high heating (cooling) rates, to achieve high temperature differences in different areas of the target.

In [4], molybdenum was used as a heat-resistant structural material for the manufacture of a test capsule in which experimental fuel elements based on uranium compounds for a light water nuclear reactor were tested. In this case, it is important to understand the limits of stability in the event of emergency radiation situations, which are modelled, among other things, using high-current sources of charged particles.

Given the wide range of applications for molybdenum, including in aerospace technology, the task arises of combining it with special alloys, such as Kovar [5]. One way to form a connection is to use electron beam welding. In [5], the peculiarities of changes in the mechanical characteristics of both materials due to the high-temperature effect of a low-energy beam were investigated. At the same time, an increase in electron energy can activate additional mechanisms of radiation-stimulated processes.

In [6], the properties of a molybdenum coating applied to an aluminum substrate irradiated with a high-current electron beam were investigated. As a result of irradiation, the molybdenum layer was melted and mixed with the substrate material to form the $MoAl_5$ phase. This method of surface modification resulted in increased corrosion resistance.

Usually, in electron beam melting of metals, in order to establish a specified heating and heat exchange mode on the irradiated surface, the shape of the beam trajectory on the target surface is specified [7]. The difference between a pulsed electron beam is that the shape of its projection onto the target is determined by the structure of the cathode, and the absorbed radiation dose is determined by the distribution of current density in the cross-section. This, in turn, will determine the distribution of the temperature field, and the task is to obtain information about the influence of the uneven distribution of current density in the beam cross-section on the distribution of the temperature field.

In works [8, 9], we stated the fact of modification of the structure of the surface layer of the irradiated molybdenum target, in particular the formation of micropores and the formation of a rough surface, which is reflected in the reflection coefficient in the IR range. Certain patterns in the orientation of surface relief irregularities were established, and assumptions were made about the occurrence of Bénard–Marangoni instabilities [1]. To confirm these assumptions, it is necessary to establish the patterns of surface relief formation in different areas of the target and determine the effect of irradiation on mechanical properties and structural-phase state.

METHODOLOGY OF EXPERIMENT

The molybdenum (purity of 99.9 wt.%) target was 1 mm thick, it was irradiated with an electron beam with a diameter of 60 mm, the electron energy was 350 keV, the pulse front duration was 5 µs, the average current during the pulse front was 2 kA. Irradiation of alloy plates was performed by a high-current pulsed beam of relativistic electrons at the TEMP-A accelerator at the National Science Center “Kharkiv Institute of Physics and Technology”. The distribution of the electron beam current density in the cross section reflected the features of the cathode shape. Metallographic analysis was performed on an IE-200 microscope. To distinguish grains, the sample was subjected to preliminary chemical treatment by boiling for 300 s in an aqueous solution of hydrogen peroxide (30%). X-ray structural analysis was performed on a DRON-4 diffractometer in copper radiation. Deciphering of the diffractograms was performed in the Match!4 program (updated crystallographic database – summer 2025). Microhardness measurement was carried out on the PMT-3 device with a load of 20 g. Fragments of fractures of the near-surface layer of the sample were examined using a scanning electron microscope JEOL-840.

For the numerical implementation of the equation, the finite difference method (FDM) with an explicit time scheme was used, which provides sufficient accuracy and stability at time steps $\Delta t = 10\,ns$ and spatial discretization $\Delta r = 100\,\mu m, \Delta z = 2\,\mu m$.

Three-dimensional visualization of the distribution $T(r,z)$ was used to analyse the spatio-temporal evolution of the temperature. Numerical arrays in the NumPy library and Matplotlib visualisation tools in Python were used to construct and process the data.

DISCUSSION OF RESULTS

Irradiation of the molybdenum surface with a high-current electron beam (HCEB) caused the formation of a wave-like relief with hemispherical protrusions (Fig. 1). The formation of such a relief is due to a series of processes during the pulse and the subsequent time interval during which the substance transitions to the solid phase as it cools below the temperature of solid-state phase transformations. Since the specific power is about 10^{12} W/cm^2 and is sufficient to melt the target, it is correct to speak of radiation-thermal mechanisms in the target, since the radiation defects formed, such as interstitial and vacancy defects, will annihilate even in the part of the target that has not been melted. Pulsed radiation exposure will primarily cause the generation of mechanical effects, which will occur due to the thermoelastic effect and reactive recoil as a result of ablation ejection of matter [10]. The occurrence of pulsed mechanical effects causes compression-rarefaction waves in the depth of the target, which, when the temperature decreases, fix internal stresses, leading to pronounced delamination when the target breaks Fig. 2.

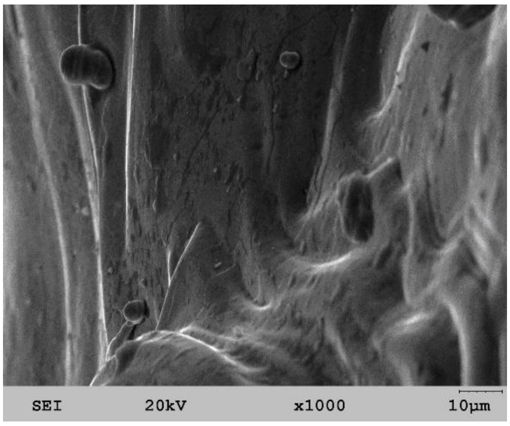

Fig. 1. SEM image of the irradiated molybdenum target area

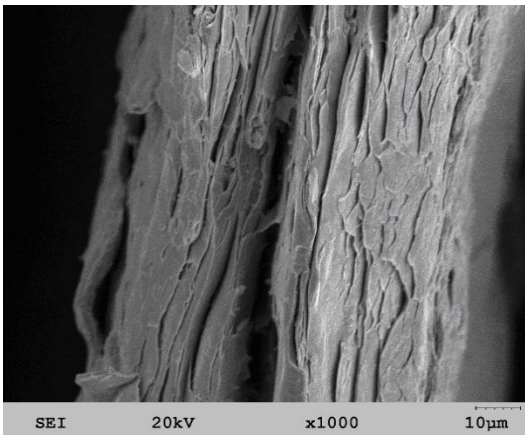

Fig. 2. SEM image of the zone of internal stress release

Fig. 3,a shows a cross-section of a molybdenum plate after HCEB treatment. The upper layer in this figure was remelted by HCEB. The average depth of the remelted (*or perhaps recrystallized)* layer is approximately $25 \ldots 30$ μm . As can be seen in Fig. 3,a, the remelted layer consists of columnar crystallites with a width of 5 to 12 μm and a height corresponding to almost the entire depth of the remelted layer. Fig. 3,b shows an enlarged fragment of the irradiated surface. As can be seen from this figure, after HCEB treatment, the clarity of most grain boundaries on the target surface is quite obvious even without etching. That is, after electron beam irradiation, grain boundaries appeared on the recrystallized surface without etching. The appearance of grain boundaries on the irradiated surface is probably caused by ultra-rapid heating and cooling during electron beam irradiation. It should be noted that the average grain size on the irradiated surface coincides with the width of the columnar crystallites in Fig. 3,a. The fact that the microstructure of treated HCEB samples can be observed directly without chemical etching has been reported earlier in works [11-13].

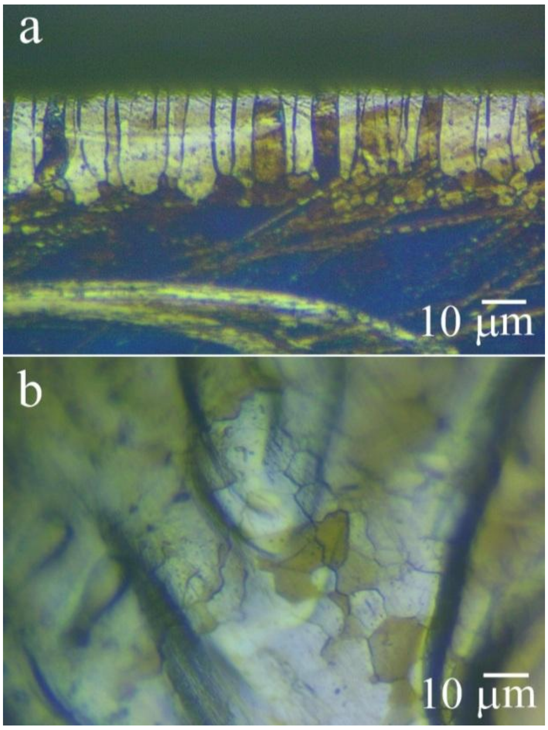

Fig. 3. Cross-section of a molybdenum plate in the electron beam treatment zone (a); view of the irradiated molybdenum surface (b). Optical microscopy

One of the features of HCEB treatment compared to other conventional surface treatment methods is the formation of a surface-modified layer with a submicroscopic crystal structure, which has a strong metallurgical bond with the unmelted part of the sample (substrate) [14]. In general, this phenomenon is caused by the rapid solidification of the molten layer under conditions of high temperature gradients and high pressures. Such conditions lead to directional crystallization of the melt under non-equilibrium conditions and can result in the formation of fine-grained and even nanocrystalline and amorphous structures [15-17]. That is, in the surface remelted layer, as a result of pulsed electron irradiation, favorable conditions are created for the dispersion of the grain structure, even if the material had a coarse-grained structure in its initial state. At the same time, the formation of a fine-grained structure after HCEB irradiation is characteristic of both various alloys and pure metals [18]. However, such grain refinement in the irradiated HCPEB zone does not always occur. There are a number of studies [19, 20], which showed that after irradiation with a pulsed electron beam, a fairly coarse-grained microstructure was formed in the surface layer treated with HCPEB irradiation. The formation of very large grains in the remelted irradiation layer in the works [19-21] is explained by the authors in terms of epitaxial growth of molten liquid from the substrate. That is, the grown epitaxial layer repeats the structure and crystallographic orientation of the substrate. In order for such epitaxial growth to occur, it is primarily important to avoid the nucleation of new grains at the solid/liquid phase boundary during solidification. The lateral size of these epitaxially grown grains, as well as their crystallographic orientation, are directly inherited from their subsurface precursors. Since pure molybdenum without impurities and dissolved gases was chosen for the study, the number of heterogeneous centers for grain nucleation during crystallization is smaller than for multicomponent alloys and steels. Another factor that can disrupt the process of epitaxial grain growth and cause the nucleation of new grains is the formation of surface ejected craters [20]. However, there are almost no pronounced crater structures on the irradiated molybdenum surface. The absence of craters on the irradiated HCPEB surface of molybdenum can be explained in terms of the crater formation mechanism proposed in [22]. According to this mechanism, craters are formed during crystallization due to chemical heterogeneity in the crystallizing layer. Since molybdenum in this study is a fairly pure metal, the probability of chemical inhomogeneities in the irradiated molten layer is very low.

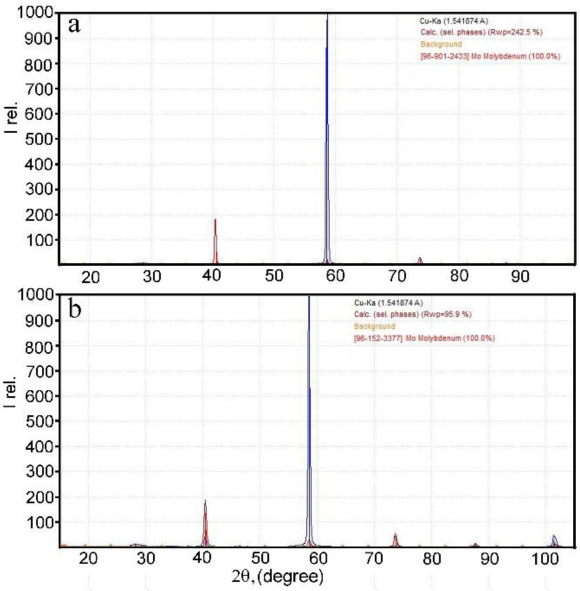

Fig. 4. X-ray diffraction patterns of molybdenum before (a) and after (b) HCEB irradiation

Based on the results of diffractometric studies, Fig. 4,a shows a fragment of the diffractogram of a molybdenum sample in its initial state. To assess the possible presence of crystallographic texture, the relative intensities of the main reflections were compared with those specified in the JCPDS-ICDD database [23], file 42-1120, and correspond to material with randomly oriented grains. The comparison results show that the Mo used in these experiments differs from the standard, i.e., it has a certain crystallographic texture. In particular, the relative intensity of the {200} peak is significantly higher than that of the standard. The results of X-ray analysis of molybdenum after HCPEB treatment are shown in Fig. 4,b. A comparison of the diffractograms in Fig. 4a and Fig. 4,b shows that these diffractograms do not differ significantly, i.e. they are almost identical. Thus, we can say that the crystallographic texture that was present in the initial state of the molybdenum samples is the same in the remelted layer. This may be evidence that the formation of a columnar green microstructure during the crystallization of the HCPEB-irradiated molten molybdenum layer occurred through the mechanism of epitaxial grain growth. An expansion of the molybdenum peaks is also observed in the remelted layer. This may be caused by the presence of second-order microstresses in the microstructure of the remelted layer.

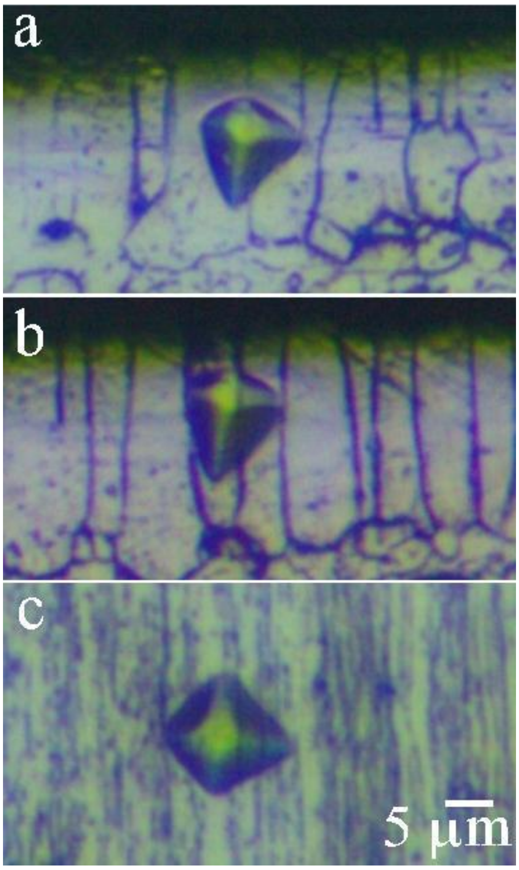

Fig. 5. Indenter impressions for measuring microhardness on cross sections of a molybdenum plate: a, b – remelted layer; c – unremelted part

The modifying effect of HCEB irradiation consists in changing the physical and technological properties of the irradiated surface layer. In this sense, an important characteristic is the microhardness of the irradiated surface. As a rule, the change in microhardness of the surface layers of metals and alloys after HCPEB treatment is ambiguous. Microhardness values may remain unchanged, increase or decrease [24, 25]. This behavior of microhardness is explained by the accumulation of point and linear defects and changes in the phase composition of the irradiated material surface. In this study, the microhardness values of molybdenum were determined by measurements on cross sections of a molybdenum plate irradiated with HCPEB. Some indenter impressions for measuring microhardness on cross sections of the remelted molybdenum layer are shown in Fig. 5,a,b, and on the non-remelted part in Fig. 5,c. The average microhardness values were determined from 10 measurements. It was found that the microhardness of molybdenum in its initial state is 168HV. The microhardness of the molybdenum layer modified by irradiation increased slightly and averaged 180HV. Thus, it was established that as a result of HCPEB exposure, the surface layer of molybdenum is strengthened, which is characterized by an increase in its microhardness by 7% compared to the initial state.

Hardness is the resistance of a material to local plastic deformation that occurs when a harder body is immersed in it. It should be noted that knowing the hardness value, conclusions can be drawn about the strength and plasticity of the material. Plastic deformation in determining microhardness is mainly carried out due to the movement of dislocations. When dislocations encounter an obstacle in their path, their sliding can no longer continue in the same way as before. The more obstacles to the movement of dislocations there are in the material, the higher the microhardness of this material will be. A number of mechanisms are responsible for increasing or decreasing microhardness: grain boundary, dispersion, solid solution and dislocation. Since pure molybdenum is being studied, and since no fine-grained structure is formed in the remelted layer, the increase in microhardness can only be due to the dislocation mechanism. That is, the only obstacle to the movement of dislocations will be other dislocations. Thus, ultra-rapid cooling generates an intense stress field in the crystallizing layer. In general, the relaxation of these stresses can be achieved by various mechanisms [26]. However, since we are talking about pure molybdenum, the main mechanism will be dislocation slip [27], due to which the dislocation density in the remelted layer will increase, which manifests itself in an increase in the microhardness of the irradiated HCPEB layer of molybdenum.

The wave-like nature of the curvature distribution on the target surface is noteworthy, demonstrating a trend toward changes in the spatial period of reproducibility and the sizes of ordered structures (Fig. 6).

The irradiation intensity decreased from the upper right corner to the lower left corner.Obviously, this is a ‘frozen’ reflection of the course of nonlinear processes in the vapor-liquid phases of the substance, which were formed as a result of irradiation.

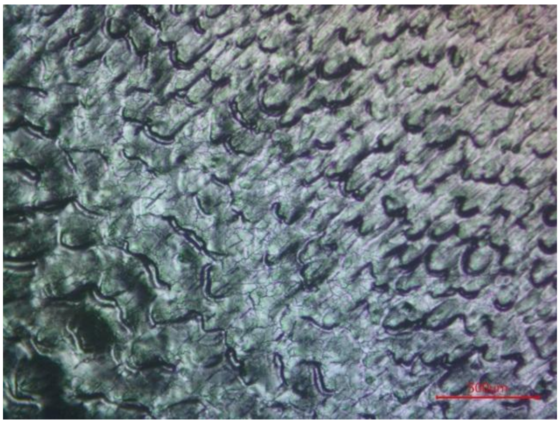

Fig. 6. Panoramic image of the target surface. Optical microscopy

The temperature field was calculated within the framework of a non-stationary heat transfer model in a cylindrical coordinate system. We assume that there is axial symmetry and no dependence on the angle. The temperature distribution is described by the heat conduction equation with an internal heat source in the form of absorbed electron beam energy:

$$\rho(T)c(T)\frac{\partial T}{\partial t} = \frac{1}{r}\frac{\partial}{\partial r}\left(rk(T)\frac{\partial T}{\partial r}\right) + \\ +\frac{\partial}{\partial z}\left(k(T)\frac{\partial T}{\partial z}\right) + Q(r,z,t) - \frac{\partial E_{ph}}{\partial t}, \quad (1)$$

$$E_{ph} = L * \rho(T) * h(T - T_m), \quad (2)$$

$$h(T - T_m) = \begin{cases} 0, T \neq T_m \\ 1, T = T_m \end{cases}, \quad (3)$$

where $\rho(T)$ is the density of the material; $c(T)$ is the heat capacity; $k(T)$ is the thermal conductivity coefficient; $Q(r,z,t)$ is the volumetric power density of the heat source caused by the absorption of energy by the electron beam; E_{ph} is a term related to the heat absorption energy during melting; $T_m = 2896$ K is the melting temperature.

The temperature dependencies of the thermophysical properties of molybdenum $\rho(T)$, $c(T)$, and $k(T)$ were obtained based on the MPDB (Material Property Database), which provides consistent values of physical constants over a wide temperature range.

This model only takes into account thermal conductivity in the solid and liquid states. Evaporation, ablation of material from the surface, and radiation heat losses were not considered.

The absorbed energy of the electron beam was distributed according to a Gaussian distribution, and the distribution of the absorbed energy of the electron beam in depth was described by a generalised analytical approximation based on the theory of penetration and energy losses of electrons in solid targets proposed by Kanaya and Okayama [28]. Within the framework of this theory, the dependence of the absorbed dose Q(x) on the normalised depth $x = z/z_m$ is as follows:

$$Q(x) = \frac{1}{(1-x)^{\frac{2}{5}}} e^{-\frac{\gamma x}{1-x}} \left(\frac{\gamma}{1-x} + \frac{3}{5}\right) \\ +2.28\frac{E_B}{E_0}\frac{\gamma}{(1-x)^2} e^{-\frac{1.9\gamma x}{1-x}} \times \left(\frac{1}{2^{5/6}} - (1-x)^{5/6}\right), \quad (4)$$

$$\gamma = z_m/z_D - 1, \quad (5)$$

where $z_D = 34$ μm is the diffusion depth of electron penetration, $z_m = 110\ \mu m$ is the maximum depth of electron penetration, found experimentally, and $E_B/E_0 = 0.7$ is the ratio of the average energy of reflected electrons to the energy of primary electrons, which was taken from [29].

Energy absorption was considered uniform within the beam radius and uniform in time during a pulse lasting up to 5 μs. At the same time, the source power was normalized so that the integral energy introduced into the system corresponded to the product of the electron energy and the beam current. The power was distributed over the beam's range of action, which was determined by the beam radius R and the maximum penetration depth of electrons z_m. Fig. 7 shows the spatial distribution of temperature after the end of the pulse, i.e. after 5 μs.

As we can see from Fig. 7, the maximum temperature value is observed in the subsurface layer, which stimulates the movement of matter towards the surface, while at the same time there is a pronounced gradient from the beam axis to the periphery, which can cause the movement of matter along the surface. This situation leads to the emergence of competing processes of dissipative structure formation by various instability mechanisms, the initiation of which is a type of second-order phase transition that requires separate study.

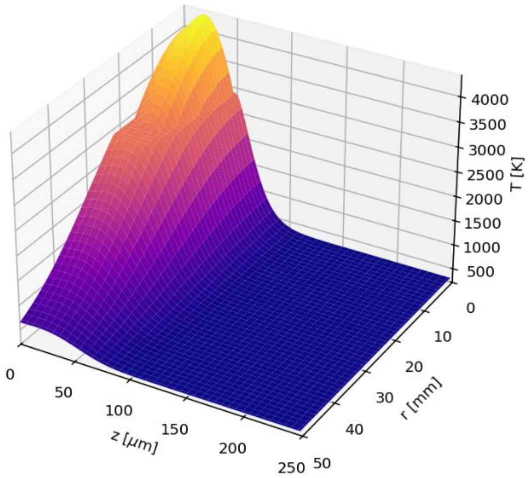

Fig. 7. Temperature distribution in the target after the end of the irradiation pulse (z – target depth, r – radius relative to the beam axis)

CONCLUSIONS

1. The effect of HCPEB on a molybdenum plate leads to melting of the surface layer and a change in the topographic pattern of the surface. The newly formed surface has a wavy pattern with hemispherical protrusions, which demonstrate a trend toward changes in the period of reproducibility and dimensions, caused by the uneven spatial distribution of the temperature field.

2. The surface layer remelted by irradiation consists of columnar crystallites up to 12 μm wide, the height of which corresponds to almost the entire depth of the remelted layer. After HCEB treatment, the clarity of most grain boundaries on the target surface is quite evident even without etching. The grain size on the

irradiated surface corresponds on average to the width of the columnar crystallites.

3. The formation of a columnar grain microstructure during the crystallization of the HCEB-irradiated molybdenum layer occurred through the mechanism of epitaxial grain growth.

4. It has been established that HCEB exposure results in the strengthening of the surface layer of molybdenum, which is characterized by a 7% increase in its microhardness compared to the initial state. The increase in microhardness of the irradiated HCEB molybdenum layer is caused by an increase in the density of dislocations that arise due to the relaxation of internal stresses during the crystallization of the molten irradiated surface layer.

ACKNOWLEDGEMENTS

The research presented in this article was financially supported by the Simons Foundation International Programme: PD-Ukraine: President Directed - Ukraine Support Grants, Record ID: SFI-PD-Ukraine-00014584.

REFERENCES

1. L. Zhang, X. Zhang, N. Li, P. Zhang, X. Mei1, Y. Wang, V.V. Uglov. Experimental and simulation studies on damage mechanisms of tungsten and molybdenum under compressed plasma flow irradiation // *Nucl. Fusion.* 2023, v. 63(7), p. 076010; https://doi.org/10.1088/1741-4326/acd016

2. N. Simos, E. Quaranta, N. Charitonidis, S. Redaelli et al. Proton Irradiation Effects on the Physio-Mechanical Properties and Microstructure of Cold-Worked Molybdenum // *J. Nucl. Energy Sci. Power Gener. Tech.* 2017, v. 6(4), p. 1000180; DOI: 10.4172/2325-9809.1000180

3. M. Virgo, S. Chemerisov, R. Gromov, C. Jonah, and G.F. Vandegrift. *Results of Thermal Test of Metallic Molybdenum Disk Target and Fast Acting Valve Testing.*ANL: Report ANL/NE-16/44. Argonne National Laboratory, 2016, 48 p.

4. C.M. Petrie, J.R. Burns, R.N. Morris, R. Smith, A.G. Le Coq, K.A. Terrani. *Irradiation of Miniature Fuel Specimens in the High Flux Isotope Reactor*: Report ORNL/SR-2018/874 Oak Ridge National Laboratory. 2018, 37 p.

5. Q. Yin, G. Chen, Y. Ma, B. Zhang, Y. Huang, Z. Dong, J. Cao. Strengthening mechanism for high-entropic weld of molybdenum/Kovar alloy electron beam welded joint // *Materials Science and Engineering.* 2022, v. A851, p. 143619; https://doi.org/10.1016/j.msea.2022.143619

6. H. Xia, C. Zhang, P. Lv, J. Cai, Y. Jin, Q. Guan. Surface alloying of aluminum with molybdenum by high-current pulsed electron beam // *Nuclear Instruments and Methods in Physics Research.* 2018, v. *B*416, p. 9-15; https://doi.org/10.1016/j.nimb.2017.11.028

7. S. Valkov, M. Ormanova, P. Petrov. Electron-beam surface treatment of Metals and Alloys: Techniques and Trends // *Metals.* 2020, v. 10, p. 1219; doi:10.3390/met10091219

8. S.E. Donets, V.V. Lytvynenko, Yu.F. Lonin, A.G. Ponomarev, et al. Behavior of molybdenum target in condition of irradiation by the high current relativistic electron beam // *Problems of Atomic Science and Technology*. 2018, N 6(118), p. 229-232.

9. S.E. Donets, V.V. Lytvynenko, O.L. Rak, V.V. Shatov, A.R. Shymanovskyi. Estimation of the effect of high-current electron beam irradiation on the radiative heat transfer modes on the molybdenum target // *Problems of Atomic Science and Technology*. 2025, N 5(159), p. 45-49; https://doi.org/10.46813/2025-159-045

10. A.G. Kobets, P.R. Horodek, V.V. Lytvynenko, et al. Melting Effects of High_Current Relativistic Electron Beam on Aluminum Alloy 1933 // *Surf. Eng. and Appl. Electrochem*. 2015, v. 51(5), p. 478-482; DOI:10.3103/S1068375515050075

11. S. Hao, P. Wu, J. Zou, T. Grosdidier, C. Dong. Microstructure evolution occurring in the modified surface of 316L stainless steel under high current pulsed electron beam treatment // *Applied surface science*. 2007, v. 253(12), p. 5349-5354; https://doi.org/10.1016/j.apsusc.2006.12.011

12. V.V. Bryukhovetsky, V.F. Klepikov, V.V. Lytvynenko, D.E. Myla, Yu.F. Lonin, A.G. Ponomarev. The Structural Phase State and Strength Properties of the Surface Layer of AA6111-T4 Aluminum Alloy Irradiated by the High-Current Electron Beam // *Nuclear Inst. and Methods in Physics Research B.* 2022, v. 519, p. 1-8; https://doi.org/10.1016/j.nimb.2022.03.008

13. D.E. Myla, V.V. Bryukhovetsky, V.V. Lytvynenko, S.I. Petrushenko, O.O. Nevgasimov, Yu.F. Lonin, A.G. Ponomarev V.T. Uvarov. Microstructure and property modifications in surface layers of a AA6111 aluminum alloy induced by high-current pulsed relativistic electron beam // *Problems of Atomic Science and Technology*. 2022, N 2(138), p. 25-31; https://doi.org/10.46813/2022-138-025

14. D.I. Proskurovsky, V.P. Rotshtein, G.E. Ozur, A.B. Markov, D.S. Nazarov, V.A. Shulov, Y.F. Ivanov, R.G.Buchheit. Pulsed electron-beam technology for surface modification of metallic materials // *Journal of Vacuum Science and Technology*. 1998, v. A16, p. 2480-2488.

15. V.V. Bryukhovetsky, V.F. Klepikov, V.V. Lytvynenko, D.E. Myla, V.P. Poyda, A.V. Poyda, V.T. Uvarov, Yu.F. Lonin, A.G. Ponomarev. The features of the structural state and phase composition of the surface layer of aluminum alloy Al-Mg-Cu-Zn-Zr irradiated by the high current electron beam // *Nuclear Inst. and Methods in Physics Research B*. 2021, v. 499, p. 25-31; https://doi.org/10.1016/j.nimb.2021.02.011

16. B. Gao, L. Hu, S.-w. Li, Y. Hao, Y.-d. Zhang, G.-f. Tu, T. Grosdidier. Study on the Nanostructure Formation Mechanism of Hypereutectic Al-17.5Si Alloy Induced by High Current Pulsed Electron Beam // *Applied Surface Science*. 2015, v. 346, p. 147-157; https://doi.org/10.1016/j.apsusc.2015.04.029

17. D.E. Myla, V.V. Bryukhovetsky, V.V. Lytvynenko, V.P. Poyda, A.V. Poyda, V.F. Klepikov, V.T. Uvarov, Yu.F. Lonin, A.G. Ponomarev. Analysis of changes in the phase and structural state of the surface layer of an aluminum alloy 1933, melted by a

pulsed electron beam // *Problems of Atomic Science and Technology*. 2020, N 2(126), p. 33-38.

18. C. Zhang, Y. Zhang, N. Tian, S. Chen, Z. Qian, P. Lv, Q. Guan. Microstructures of pure nickel induced by high-current pulsed electron beam irradiation //*Protection of Metals and Physical Chemistry of Surfaces*. 2016, v. 52, p. 869-875; https://doi.org/10.1134/S2070205116050269

19. Y. Samih, G. Marcos, N. Stein, N. Allain, E. Fleury, C. Dong, T. Grosdidier. Microstructure modifications and associated hardness and corrosion improvements in the AISI 420 martensitic stainless steel treated by High Current Pulsed Electron Beam (HCPEB) // *Surface and Coatings Technology*. 2014, v. 259, p. 737-745.

20. P. Yan, T. Grosdidier, X. Zhang, J. Zou. Formation of large grains by epitaxial and abnormal growth at the surface of pulsed electron beam treated metallic samples // *Materials and Design*. 2018, v. 159, p. 1-10.

21. Y. Sun, K. Li, B. Gao, P. Sun, H. Fu, Z. Liu, J. Yin. Study on microstructure and wear resistance of Zr-17Nb alloy irradiated by high current pulsed electron beam // *Reviews on Advanced Materials Science*. 2020, v. 59(1), p. 514-522.

22. V.V. Bryukhovetsky, V.F. Klepikov, V.V. Lytvynenko, D.E. Myla, O.A. Startsev, Yu.F. Lonin, A.G. Ponomarev. Formation mechanism of craters on the surface of AA6111 aluminum alloy irradiated by quasi-relativistic high-current electron beam // *Vacuum*. 2023, v. 215, p. 112263; https://doi.org/10.1016/j.vacuum.2023.112263

23. International Centre for Difraction Data; JCPDS: Newtown Square, PA, USA, 1907.

24. Y. Qin, C. Dong, Z. Song, S. Hao, X. Me, J. Li, X. Wang, J. Zou, Th. Grosdidier. Deep Modification of materials by thermal stress wave generated by irradiation of highcurrent pulsed electron beams // *Journal of Vacuum Science and Technology A*. 2009, v. 27(3), p. 430-435.

25. V.V. Bryukhovetsky, V.V. Lytvynenko, D.E. Myla, V.A. Bychko, Yu.F. Lonin, A.G. Ponomarev, V.T. Uvarov. Effect of Structural and Phase Changes under Relativistic Electron Pulsed Beam Irradiation on the Aluminum Alloys Micro-hardness // *Physics and Chemistry of Solid State*. 2021, N 22(4), p. 655-663; doi.org/10.15330/pcss.22.4.655-663

26. V.V. Bryukhovetsky, V.V. Lytvynenko, O.A. Startsev, D.E. Myla, Yu.N. Volkov, O.L. Rak. Mechanisms of deformation induced by high-current pulsed electron beam irradiation // *Materials Letters*. 2024, v. 367, p. 136642; https://doi.org/10.1016/j.matlet.2024.136642

27. K.M. Zhang, J.X. Zou, B. Bolle, T. Grosdidier. Evolution of residual stress states in surface layers of an AISI D2 steel treated by low energy high current pulsed electron beam // *Vacuum*. 2013, v. 87, p. 60-68; https://doi.org/10.1016/j.vacuum.2012.03.061

28. K. Kanaya, S. Okayama. Penetration and energy-loss theory of electrons in solid targets // *Journal of Physics D: Applied Physics*. 1972, v. 5(1), p. 43; DOI: 10.1088/0022-3727/5/1/308

29. L. Yang, A. Hussain, S. Mao, Bo Da, K. Tőkési, Z.J. Ding. Electron backscattering coefficients of molybdenum and tungsten based on the Monte Carlo simulations // *Journal of Nuclear Materials.* 2021, v. *553*, p. 153042; https://doi.org/10.1016/j.jnucmat.2021.153042

Article received 15.11.2025

СТРУКТУРНО-ФАЗОВІ ПЕРЕТВОРЕННЯ В МОЛІБДЕНОВІЙ МІШЕНІ ПІД ВПЛИВОМ ВИСОКОПОТУЖНОГО ПУЧКА ЕЛЕКТРОНІВ

В.В. Брюховецький, С.Є. Донець, С.А. Князєв, О.В. Суббoтін, В.В. Литвиненко, С.І. Богатиренко, О.Л. Рак, А.Р. Шимановський

Вивчаються особливості поверхневого рельєфу, будови і орієнтації зерен приповерхневого шару, структурно-фазового складу, мікротвердості молібденової мішені, що була опромінена сильнострумовим імпульсним електронним пучком (НСЕВ). Встановлено ефект формування стовпчастої зеренної приповерхневої мікроструктури шляхом епітаксіального росту з підкладки. Проведено моделювання розподілу температурного поля, показано, що температурні градієнти вздовж поверхні зумовлюють виникнення нестійкостей розплавленого шару, які зумовлюють формування дисипативних структур.